New Folder Name The Rigid inline-modulated Interferometer at MIT

LIGO-T900009-00-R

#96

List of 5/23/90

The rigid inline-modulated interferometer at MIT:
A summary of results

P. Fritschel, D. Shoemaker, R. Weiss

27 March 1990

Introduction

This report describes the rigid, internally-modulated Michelson interferometer with Fabry-Perot cavities at the MIT laboratory. The optical layout and the measurements of losses and contrast are given; the servo systems are described; and the signal and noise characteristics are discussed.

Optics

Layout: The layout is shown in figure 1. The interferometer is constructed with commercial mirror mounts on small optical tables bolted to the circular bottom plate of the 1.5 m diameter central tank of the MIT 5 m prototype vacuum system. This bottom plate is isolated from seismic ground motion with rubber-damped springs, giving horizontal and vertical resonances of $\approx$4 Hz. The vacuum tank is closed, but not pumped down, during the experiment. The entire tank is overpressured with filtered air; the cavity mirrors and the space between them are protected by glass tubes filled with very clean (filtered to 0.1 μ with 99.99% efficiency) boil-off from liquid N_2 or with He gas. Sound absorbing material (Sonex 1) inside the tank is used to absorb acoustic noise.

The light from the laser (which is on a separate table) is coupled into a single-mode fiber, and this fiber is led into the vacuum system and is terminated in the block labeled 'fiber-grin'; the output of this fiber-grin lens assembly is a nearly collimated beam. It is mode-matched to the Fabry-Perot (FP) cavities with a single positive lens, and isolated by two Faraday isolators in series. The light falls on a disk beam-splitter labeled BS and is sent (in each arm) through a Pockels cell (**PCA** and **PCB** in the figure) and into the 47 cm long FP cavity. A small part (3%) of the reflected light is sent to a photodiode (**PDA** or **PDB**); the rest returns to the beam-splitter where it interferes with the light from the other arm. The light leaving the anti-symmetric port of the interferometer falls on the third photodiode **PDC** in the system. The light leaving the interferometer through the symmetric port (coincident with the incoming light) is rejected by the middle polarizing beamsplitter in the Faraday-isolator assembly.

Measured optical characteristics: The Ar^+ laser (*Spectra-Physics 2020*) has a selective output coupler for the 514.5 nm line and an étalon for single longitudinal-mode operation. With the intra-cavity Pockels cell which is used for the frequency stabilization, the laser has about 0.5 W maximum output (0.85 W without Pockels cell). The overall optical efficiency of the light delivery system is 0.3 (0.5 from the fiber coupler; 0.6 from the assorted lenses and Faraday isolators).

The FP cavities themselves are made up of mirrors polished by Optics Technology and coated by PMS. The input coupling mirror is flat, and the rear mirror has a 1 m radius.

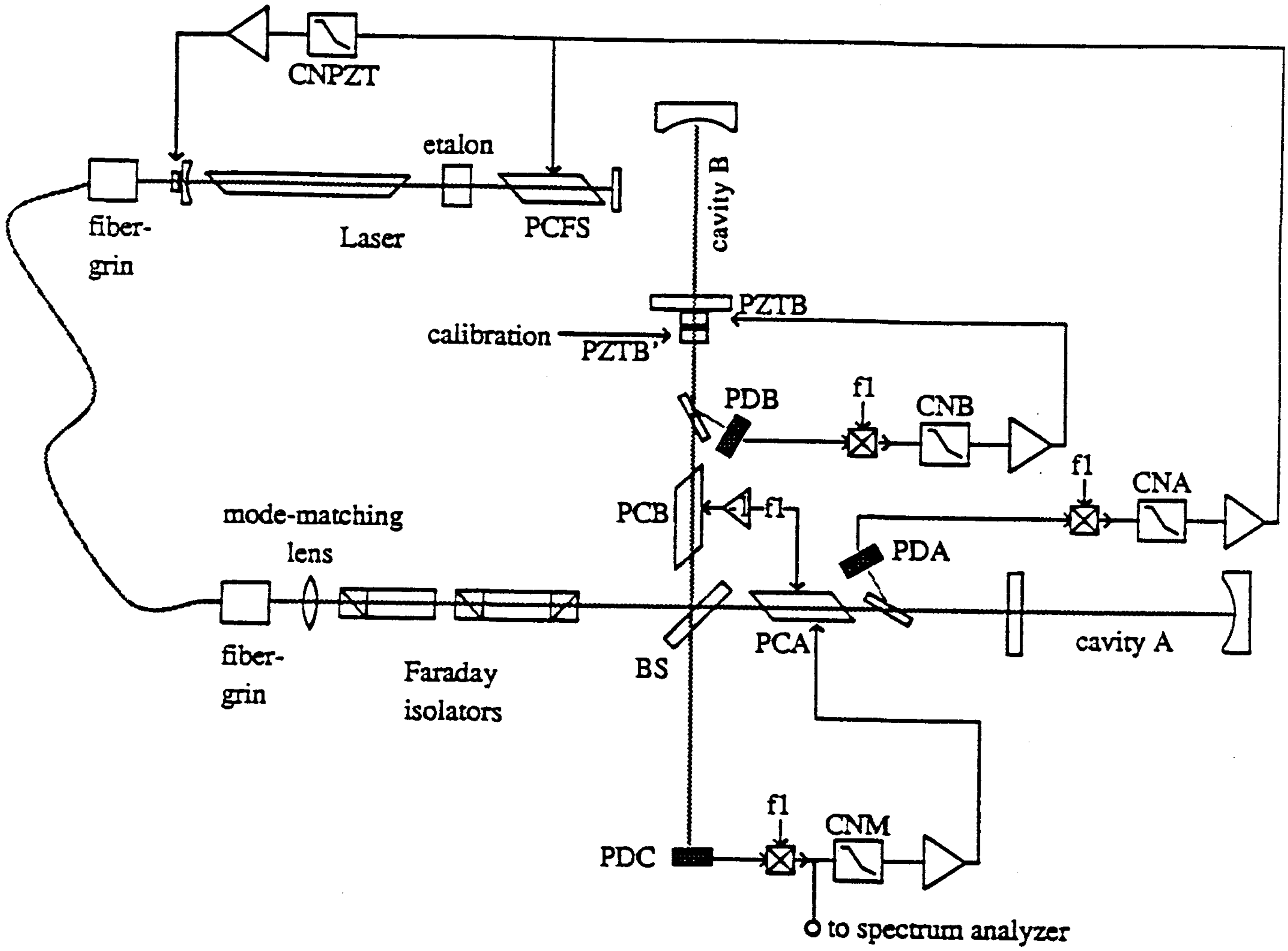

Figure 1: Schematic diagram of the interferometer.

The transmission of the input coupling mirror is 2.8%, and thus the finesse is about 220, and the linewidth 1.4 MHz. By looking at the transmitted light though the cavity as it is swept in length through a free spectral range, the mode matching can be determined: the intensity of the light in the TEM_{00} mode can be compared with the sum of the intensities in all of the modes. This gives a mode matching efficiency of 95%. The reflectivity of the cavity on resonance is 97.5% (corrected for the finite matching), which allows us to infer the total losses in the cavity to be 160 ppm. PMS had quoted losses for the rear mirror of 52 ppm (of which 17 ppm are due to transmission), and thus we believe that the input coupling mirror has losses of the order of 110 ppm. To the precision of our measurements (roughly 5%), we see no difference between the two cavities in terms of the matching, finesse, or losses. We have seen no degradation of the mirror characteristics over a one month period, and thus our precautions in providing a clean environment appear to be sufficient.

The far mirrors of the FP's can be blocked, leaving a simple Michelson interferometer (MI). The contrast of this interferometer, *without* Pockels cells in place, is $C = (I_{max} - I_{min})/(I_{max} + I_{min}) = 0.996$; *with* the Pockels cells (Gsänger PM-25) in place, the contrast becomes $C = 0.989$ (which we believe is primarily due to one particular Pockels cell which shows excessive scattering). With the FP cavities locked, the contrast is $C = 0.986$. This last figure may be limited by our present ability to align the system; remote controls (PZT's) and misalignment information (phase front analysis) will be necessary to determine the intrinsic limits.

Servo- and measurement systems

Synchronous detection at $f1$=5.38 MHz is used to detect the lengths of the two cavities (via the reflected light) and the Michelson fringe (via the light leaving the anti-symmetric port). The modulation is impressed on the laser light by the Pockels cell in each arm (**PCA**, **PCB**) of the interferometer. The laser frequency is stabilized to the length of cavity 'A'; the cavity 'B' is held on resonance via an actuator **PZTB** mounted on one of the cavity mirrors; and the Michelson is held on the dark fringe through voltages applied (in addition to the modulation) to the Pockels cells.

Frequency stabilization: The laser is stabilized to the cavity 'A', using the reflection technique. The error signal is derived by demodulating a fraction of the reflected light with 5.38 MHz. It is sent through a servo compensation network **CNA**, which is a simple pole at 100 Hz for the initial locking; for normal operation, another pole-zero pair (100 Hz-100 kHz) is used. Finally, a Sallen-Key circuit can be added to give extra gain in the vicinity of 80 kHz (at the expense of a reduced gain around 40 kHz). The signal is amplified by an Inrad high-frequency high-voltage (±85 V) amplifier and applied to a Pockels cell **PCFS** in the laser cavity. The unity-gain frequency is about 700 kHz with a simple pole as compensation; with the normal compensation filter in place, the unity-gain frequency is $\approx$300 kHz. Long-term drifts are countered by a second loop (with compensation **CNPZT**) using a PZT actuator on the laser output coupling mirror.

Arm 'B' cavity locking: The second arm is locked to the stabilized laser light frequency with the same reflection and demodulation technique as above. The basic servo compensation **CNB** is similar to that for cavity 'A', except that the pole/zero pair for the normal operating condition is at 1 Hz-3 kHz. The actuator for the servo-system is a PZT **PZTB** on the input coupling mirror of cavity 'B', which has a pronounced (24 kHz, Q=15) resonance; to allow a higher unity gain frequency in the servo-loop, a passive anti-resonance circuit in the compensation network **CNB** is used to cancel this resonance. The unity-gain frequency thus achieved is 4.5 kHz, which is sufficient to make the excursions from the cavity resonance acceptably small.

With the normal light intensities used for measurements, the unity signal-to noise (shot and electronic noise limited) for the frequency detection is about 0.3 $\mathrm{Hz}/\sqrt{\mathrm{Hz}}$. For frequencies between 6 kHz and 100 kHz, the gain in the servo loop is sufficient to hold the frequency noise to less than 1 $\mathrm{Hz}/\sqrt{\mathrm{Hz}}$; with the Sallen-Key circuit in place, the frequency noise at 80 kHz is held to the shot noise limit of 0.3 Hz/$\sqrt{\text{Hz}}$. We have measured the frequency sensitivity of the complete recombined beam interferometer to be $2.5 \cdot 10^{-17}$ m/Hz; this can be interpreted as a difference in storage times of the two cavities of one part in 2000. Thus, the apparent position noise associated with this noise term is at a level of $7.5 \cdot 10^{-18}$ m/$\sqrt{\text{Hz}}$, which is somewhat below the shot noise limited position sensitivity of of the recombined beam interferometer of $2.5 \cdot 10^{-17}$ m/$\sqrt{\text{Hz}}$.

Michelson locking and detection: The Michelson path length difference is modulated by the same Pockels cells that are used to apply the modulation to the cavities. However, the level of the modulation is significantly reduced by the optical arrangement which has the light passing two times through the Pockels cells.

In the first pass through the Pockels Cells (PC), the carrier has two sidebands at $\pm f1 = \pm 5.38$ MHz put upon it. This falls on a cavity; the sidebands are largely outside of the resonance curve of the Fabry-Perot, and thus are shifted by roughly 0 and 2π upon reflection. The carrier, which is held on the cavity resonance, is shifted by π upon reflection. The reflected light now undergoes a second interaction with the modulator; new sidebands are put on the reflected carrier, which are out of phase with the sidebands that were put on in the first pass through; thus there is a cancellation of the modulation.

The quality of the cancellation is a function of several parameters. First, the visibility of the cavity fringes: in the current cavities, all but 2.5% of the light is reflected. Secondly, the linewidth of the cavity as compared with the modulation frequency: for the FP cavities, and 5.38 MHz modulation, the two reflected sidebands are not at 0° and 360° but at 13° and 360°-13°. Thirdly, the distance between the modulator and the cavity input coupling mirror: the time of transit causes an additional phase shift between the original and second sidebands (this contributes about 3° of phase delay). A calculation shows the ratio of the signal at the modulation frequency in the double-passed configuration to the signal for a single pass through the modulator to be

$$\frac{I^{double-pass}(\omega_m)}{I^{single-pass}(\omega_m)} = J_0^2(\Gamma)\,[(1-\sqrt{A})^2 + (\sin(2\omega_m l/c + \phi_{cav}))^2]^{\frac{1}{2}} \ .$$

This is derived for the case of unity contrast. Here Γ is the modulation index for a single pass through the modulator, A is the intensity reflection coefficient of the cavity on resonance, l is the distance from the modulator to the cavity, and ϕ_{cav} is the phase shift added to the $\omega_0 \pm \omega_m$ sidebands upon reflection from the cavity. In our case, the amplitude term, $(1-\sqrt{A})^2 = (1-0.987)^2 = 1.7 \cdot 10^{-4}$, is very small, and our signal comes almost entirely from the phase shift term, $(\sin(16°))^2 = 7.6 \cdot 10^{-2}$, which gives a signal ratio of $I^{d.p.}/I^{s.p} = 1/3.7$ for a typical Γ of 0.16. Our observations of this reduction compare the ω_m signal (monitored at the RF output of **PDC**) of the FP MI and the one-bounce MI. In the one-bounce MI the modulation is very nearly doubled on the second pass and we would predict a signal ratio, in the region where $J_1(\Gamma)$ is linear with Γ, of $I^{\mathrm{FPMI}}/I^{\mathrm{MI}} = 1/7.4$, which is in fair agreement with our directly observed ratio of 1/9. The result of this cancellation is that the optimum modulation depth in the recombined beam FP MI can not be reached; note that the cavity lock (for which the signal is picked off before the second pass through the modulator) does not suffer from this cancellation.

However, sufficient signal is available to hold the Michelson to a dark fringe and to make measurements of the resulting signal-to-noise ratio. The demodulated signal from the photodiode receiving the light from the antisymmetric output of the interferometer is put through a compensation network **CNM** similar to those above, with a pole at 160 Hz for initial locking and a pole-zero pair at 1Hz-3 kHz for normal operation. The filtered signal is amplified with a fast high-voltage amplifier and sent to one of the Pockels cells; a unity gain frequency of 5 kHz is attainable and sufficient. We analyze the error signal of this loop above the unity gain frequency to obtain the displacement noise spectrum. It is calibrated in displacement using a second PZT **PZTB′** mounted on the 'B' arm cavity input coupling mirror: the signal for a given applied 35 kHz signal can be seen in both the recombined-beam FP Michelson and in the simple interferometer, where the absolute magnitude can be determined either from the known sensitivity of the Pockels cell or from the calibration signal size directly compared with the Michelson output fringe amplitude.

Signal sensitivity, noise sources

Figure 2 shows the spectrum, expressed as equivalent mirror displacement noise in $\mathrm{m}/\sqrt{\mathrm{Hz}}$, for the interferometer. The photocurrent on the Michelson light fringe for these measurements is 8 mA (which corresponds to ≈35 mW of power). The top flat curve is the spectrum of the demodulated signal from the Michelson antisymmetric output of the simple one-bounce Michelson; note the lack of features at frequencies above ≈10 kHz. This noise level is at the shot noise limit for the measurement. This curve assures us that the electronic systems are working correctly.

The spectrum with the two Fabry-Perot cavities locked is the middle, rapidly falling curve in figure 2. At low frequencies (up to 30 kHz) acoustic noise is dominant. This source of noise determines the servo-loop characteristics which are required, as it is against these large fluctuations that the system must be held on resonance or on the dark fringe. In the 30 kHz to 100 kHz band, a number of resonances can be seen; these are probably thermally-driven resonances in the FP cavity mirror supports, and are consistent with masses and resonance Q's in the system. This noise source is the practical limit to the obtainable sensitivity with this interferometer constructed of mirrors in conventional mounts.

Initially, data were taken with nitrogen gas in the glass tubes protecting the mirrors. On the order of 100 resonances between 10 and 100 kHz, with Q's of 500 to 1000, dominated the spectrum; see figure 3. When the nitrogen was replaced with helium, these peaks dissapeared. Apparently, thermally driven transverse acoustic resonances of the gas in the tubes caused measurable fluctuations in the path length; this effect is much reduced in helium, which has a polarizability (proportional to n-1) roughly 10 times less than that of nitrogen for a given pressure.

In a region between 70 and 85 kHz, the spectrum closely approaches the shot noise associated with the photocurrent of the measurement (as determined by replacing the laser light on the antisymmetric photodetector with incoherent light from an incandescent light bulb, shown as the bottom trace in figure 2). This corresponds to a sensitivity of ≈ $2.5 \cdot 10^{-17}\ \mathrm{m}/\sqrt{\mathrm{Hz}}$. We note that the increase in sensitivity obtained by adding the cavities

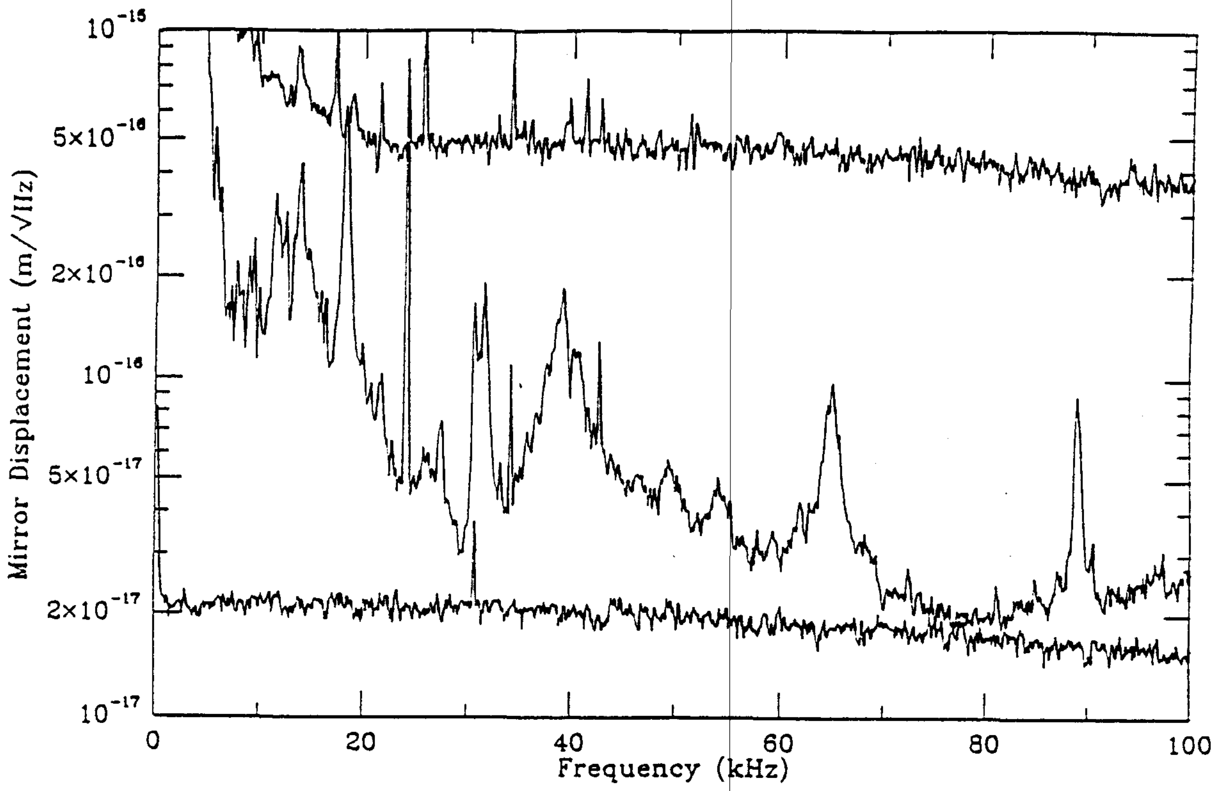

Figure 2: The interferometer spectrum. Top curve: the simple one-bounce Michelson interferometer. Middle curve: the recombined beam FP MI. Bottom curve: the shot noise for the recombined beam FP MI

---

is of the order of 25; this sensitivity is reduced from the ideal factor of 2(finesse)/π $\approx$140 due to the reduction in modulation depth discussed above.

A thorough calculation of the sensitivity of this instrument that properly takes into account contrast imperfections and the double-passing of the modulator is quite involved. However, for small modulation, where $J_1(\Gamma)$ is linear with Γ, the double-passing is approximately equivalent to reducing the modulation depth, and we can use the simple sensitivity formula for a single-passed recombined beam FP MI, replacing the single-pass modulation index with our reduced index. In the limit where the measurement frequency is small compared with the linewidth $c/2lF$ of the Fabry-Perot cavities in the arms of the interferometer, this gives for the sensitivity $\tilde{x}$, where $\tilde{x}$ is the motion of one interferometer mirror,

$$\tilde{x} = \left(\frac{\lambda}{8F}\right)\left(\frac{2e}{I_{max}}\right)^{\frac{1}{2}}\left(\frac{\sqrt{2}[J_0^2(\Gamma_{net})A(1-C)+(1-J_0(2\Gamma_{net}))]^{\frac{1}{2}}}{J_0(\Gamma_{net})J_1(\Gamma_{net})\sqrt{1+C}}\right) .$$

Here $\lambda = 0.514\cdot10^{-6}$ m is the wavelength of the light, F is the arm cavity finesse, e is the electronic charge, I_{max} is the photocurrent at the interferometer output on the bright fringe, A is the average on-resonance cavity reflection coefficient of the two cavities, and

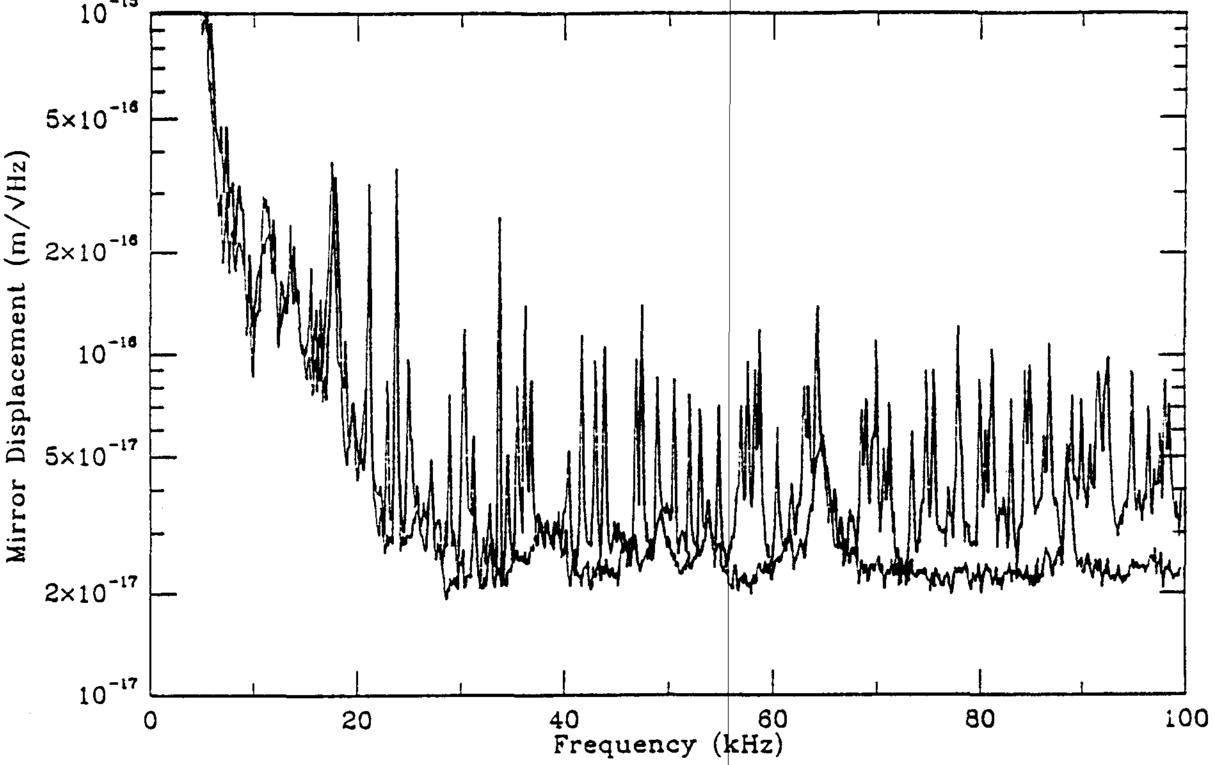

Figure 3: The interferometer spectrum, with nitrogen (top curve) and helium (bottom curve) in the tubes protecting the cavity light path and mirrors

$J_0(\Gamma)$ and $J_1(\Gamma)$ are Bessel functions; the depth of modulation Γ_{net} is the net modulation, after cancellation. The interferometer contrast, C, is modelled by a difference in the on-resonance cavity reflection coefficient for the two arms. This is probably not the most accurate model for our experiment, where the contrast defect most likely comes from power not in the TEM_{00} mode, but it is a simple model to calculate; other models give negligibly different values for the signal-to-noise ratio. The first factor in the sensitivity formula is the change in phase of the interferometer arm ϕ for a change in length x of the arm; for our cavities, with a finesse of $F = 220$, this has a value of $2.9{\cdot}10^{-10}$ m/rad. The second factor is the phase uncertainty $\tilde{\phi}$ due to the shot noise of the photocurrent. For the measurement presented here, we have I_{max} =8 mA, and $\tilde{\phi} = 6.3{\cdot}10^{-9}\mathrm{rad}/\sqrt{\mathrm{Hz}}$. These first two factors together give the ideal shot noise limited unity signal-to-noise ratio, which for the measurement presented here gives a possible sensitivity of $1.8{\cdot}10^{-18}$ $\mathrm{m}/\sqrt{\mathrm{Hz}}$. The third factor takes into account the imperfections in the optical and detection systems. Here the finite contrast ($c = 0.95$ for the measurement presented) and largely cancelled modulation ($\Gamma_{net} = 0.036$, which has been reduced by the measured factor of $I^{\mathrm{FPMI}}/I^{\mathrm{MI}} = 1/9$) give a factor of 12.6, and thus a predicted sensitivity of $2.3{\cdot}10^{-17}$ $\mathrm{m}/\sqrt{\mathrm{Hz}}$. This is in good agreement with the measured value.

In a separate experiment to verify the increase in sensitivity due to the Fabry-Perot cavities in the interferometer arms, a fixed-level 60 kHz modulation was applied to the cavity 'B' piezoelectric transducer **PZTB**. Cavity 'A' was blocked. With cavity 'B' alternately on resonance and off resonance (and thus effectively blocked), the Michelson was swept through several fringes, and the antisymmetric output was demodulated with the 60 kHz modulation frequency. The demodulated signal on resonance was 143 times greater than with the unlocked cavity, which is in excellent agreement with the expected result. This low-frequency (kHz) test, which does not suffer the reduction in modulation depth seen with higher (MHz) modulation frequencies, is a direct confirmation of the expected increase in sensitivity to arm length changes when a cavity is used.

Conclusion

We have demonstrated a Michelson interferometer with internal modulation and with Fabry-Perot cavities (with a finesse appropriate to a full-scale interferometer) in the the arms. Its optical characteristics are encouraging: the relatively small losses in the arms, the symmetry between the arms, and the high contrast between the recombined beams, indicate that some aspects of the mirror technology for the full scale interferometers are close at hand. The shot-noise limited sensitivity of the interferometer, $2.5 \cdot 10^{-17}$ m/$\sqrt{\text{Hz}}$, agrees well with the calculated sensitivity for the experimental parameters. The modulation technique that has been used here, while convenient for initial prototyping efforts, has several disadvantages, the most important being that electro-optic modulators introduce contrast defects and cannot withstand the desired power levels in recycled interferometers without introducing considerable beam distortion. In addition, the cancellation of the modulation in the Michelson reduces the sensitivity and complicates the somewhat interpretation of our experimental arrangement. A longer path length between the modulator and the cavity input mirror (of the order of 14 m for our present modulation frequency $f1$=5.38 MHz) would provide a solution to the cancellation of the modulation sidebands, but an alternative modulation scheme such as external modulation is a more attractive and complete solution.

However, the inline modulation system is a convenient starting point for recombining the beams in the 40-meter system providing that the present absorbing cavities are used in the initial setup. There is a substantial convenience in the simplicity of the scheme and the ease of phase control with the internal Pockels cells. The behavior of the inline modulation system and its signal and noise characteristics are well understood. We recommend that the inline modulation be used for the first recombination experiments on the 40-meter interferometer.